An adaptive composite discontinuous Galerkin method for elliptic problems on complicated domains with discontinuous coefficients

Stefano Giani

Department of Engineering, University of Durham, South Road, Durham DH1 3LE, UK

Abstract

In this paper, we introduce the Multi-Region Discontinuous Galerkin Composite Finite Element Method (MRDGCFEM) with hp-adaptivity for the discretization of second-order elliptic partial differential equations with discontinuous coefficients. This method allows for the approximation of problems posed on computational domains where the jumps in the diffusion coefficient form a micro-structure. Standard numerical methods could be used for such problems but the computational effort may be extremely high. Small enough elements to represent the underlying pattern in the diffusion coefficient have to be used. In contrast, the dimension of the underlying MRDGCFE space is independent of the complexity of the diffusion coefficient pattern. The key idea is that the jumps in the diffusion coefficient are no longer resolved by the mesh where the problem is solved; instead, the finite element basis (or shape) functions are adapted to the diffusion pattern allowing for much coarser meshes. In this paper, we employ hp-adaptivity on a series of test cases highlighting the practical application of the proposed numerical scheme.

Keywords: composite finite element methods, discontinuous Galerkin methods, discontinuous coefficients, adaptivity

1. Introduction

Many challenging problems in science and engineering involve partial differential equations (PDEs) with coefficients with discontinuities on a "small" scale. This is common for photonic crystals [21] and composite materials [28]. In such problems, the discontinuities of the coefficients form subregions that

could have very complicated geometries. Standard finite element methods struggle on such problems because meshes fine enough to describe the pattern of the discontinuities of the coefficients on the domain have to be used. In such situations, an extremely large number of elements may be required for a mesh generator to produce even a "coarse" mesh and the solution of the resulting system involves a large number of degrees of freedom and it is computationally very expensive.

In recent years, a new discontinuous Galerkin method referred to as Discontinuous Galerkin Composite Finite Element Method (DGCFEM) [4], has been developed for the numerical solution of partial differential equations on complicated domains characterized by small geometric details or holes. Subsequently, in [17, 16] adaptivity was added to the method and later in [14] the method was extended to eigenvalue problems. What all these incarnations of DGCFEM have in common is the focus on domains with geometries difficult to resolve using standard FEMs. Often the DGCFEM is applied to problems on domains with small details forming a small-scale structure of holes. A lot of engineering applications involve such domains. However, for other classes of problems like photonic crystal fibres and composite materials, the small-scale structure does not consist of holes, but distinct values of coefficients in the governing PDE. Discontinuities in the coefficients on a fine scale, especially for the diffusion coefficient, cannot be effectively tackled so far by the DGCFEM. This is because DGCFE coarse elements have standard polynomial spaces like $\mathbb{Q}_p$ or $\mathbb{P}_p$ defined on them, therefore standard polynomials are not able to approximate well discontinuities in the gradient of the solution within the elements. In this work, we present a way to extend the DGCFEM to overcome such difficulty.

Problems with subregions are common in physics and engineering, therefore many variations of finite element methods (FEMs) has been proposed for problems with subregions. In CutFEM [24, 10, 19, 18], a standard mesh is adjusted to fit the interface between the regions by cutting elements crossing the interface. The interface between the regions is described implicitly using a higher dimension surface, like in level-set methods [25]. The cut elements are no longer standard elements with regular shapes, therefore a new way to integrate over such shapes is added to the method. This introduces extensions to the FEM formulation to work on cut elements. In comparison, in the DGCFEM, the integration over elements of any shape can be done using standard quadrature rules on regular elements thanks to the presence of the fine level mesh [4]. Moreover, CutFEM shares similar limitations to many

level-set methods when it comes to computing the intersection between the mesh and the interface. The interface is approximated on the mesh using a piecewise linear interpolation. For the interpolation to be accurate, the interface must not be too "wiggly" inside each element. This put a constraint of the maximum size of elements that can be used and in the presence of complicated interfaces, very small elements may be needed to be able to describe accurately the interface. The method presented in this work has not such limitation allowing for elements of any size to be used. In [9], this issues is mitigated introducing a finer uniform background mesh or an adaptively refined background mesh along the interface for the quadrature rule. This removes the constraint on the size of the elements, however, the methods are still limited by the fact the interface is approximated only linearly, meaning that, for example, if the interface between the regions is a circle, such geometry can never be exactly described by the interpolated interface. In Section 5.2, such an example is considered and in our method, the interface is exactly described.

Another method that uses cut elements and implicit description of the interface is the Cut-Cell method [11, 8, 6, 27]. The Cut-Cell method can also be used with finite difference and finite volume discretisations. Also in the case of the Cut-Cell method, the interface is approximated in a piecewise linear manner leading to the same limitations already discussed for the CutFEM.

There are methods in literature with the ability to represent complex small scale geometries, Multiscale FEMs [22, 1, 2] are among the most used. Similarly to the DGCFEM, Multiscale FEMs uses special basis functions constructed to take into account the small scale features of the problem. Such construction in the Multiscale FEM setting is done by solving a series of local problems. This approach is much more computationally expensive than the projection used in the DGCFEM to accomplish the same result [4]. Furthermore, the definition of the local problems used in Multiscale FEMs depend on the PDE problem to solve, instead the DGCFE projection is PDE independent.

Another class of methods found in the literature with similar capabilities to the Multiscale FEMs are the Orthogonal Decomposition Methods [12, 20]. Also, in this case, special sets of basis functions called corrected basis functions have to be computed solving local problems which are also computationally more expensive than the projection used in the DGCFEM.

Finally, another very popular method to deal with PDEs with small-scale

3

features is homogenization [23, 3], which consist of expanding the solution of the PDE in a power series and constructing a multi-scale asymptotic expansion of the problem considering only the first few terms of the power series. The most common choice is to just use a two-scale asymptotic expansion. Homogenization has been shown to work well when the size of the entire domain is several orders of magnitude larger than the small-scale features and when the small-scale features form a periodic pattern. Therefore, there are many problems that do not possess these characteristics such as all problems that have "small" features in the meso-scale size and not in the micro-scale and problems with non-periodic features.

The structure of this article is as follows. In Section 2, we introduce the model problem and state the necessary assumptions on the computational domain Ω. Section 3 introduces the multi-region discontinuous Galerkin composite finite element spaces. In Section 3.1 we present the a priori convergence results for the method; the a posteriori error estimator used to drive the adaptivity is presented in Section 4. The performances of the MRDGCFEM on a series of test cases are studied in Section 5. Finally, in Section 6 we summarize the work presented in this paper and draw some conclusions.

2. Model problem

In this article we consider the following model problem: given $f \in L_2(\Omega)$ and $g \in H^{1/2}(\partial\Omega)$, find u such that

$$
\begin{aligned}
-\nabla \cdot (\mathcal{A}\nabla u) &= f & &\text{in } \Omega, \\
u &= g & &\text{on } \partial\Omega.
\end{aligned}
\tag{1}
$$

Here, Ω is a bounded connected polyhedral domain in $\mathbb{R}^d$, $d = 2, 3$, with boundary $\partial\Omega$ and $\mathcal{A}$ may assume a finite number of positive values in the domain Ω, with $\mathcal{A}_{\max}$ the maximum value of $\mathcal{A}$ in Ω. We also assume that Ω can be partitioned into n connected regions $\mathcal{C}_j$, with $j = 1, \ldots, n$ where the value of $\mathcal{A}$ is constant in each of them, n maybe large. We assume that these connected regions are forming a meso-structure or micro-structure. In order to define the method we group together the regions $\mathcal{C}_j$ into possibly disconnected m regions $\mathcal{R}_i$, with $m \leq n$, where the value of $\mathcal{A}$ is the same. Therefore each region $\mathcal{R}_i$ is the union of all regions $\mathcal{C}_j$ where $\mathcal{A}$ has a certain value. Along the boundaries Γ between different regions $\mathcal{R}_i$, the solution u

4

of (1) satisfies:

$$
\begin{aligned}
u^+ &= u^- \quad \text{on } \Gamma, \\
\mathcal{A}^+ \nabla u^+ \cdot \mathbf{n}^+ &= -\mathcal{A}^- \nabla u^- \cdot \mathbf{n}^- \quad \text{on } \Gamma,
\end{aligned}
\tag{2}
$$

where the superscripts $+$ and $-$ indicate the quantities from either side of the interface Γ and within the two regions indicated by $\mathcal{R}^+$ and $\mathcal{R}^-$. The vectors $\mathbf{n}^+$ and $\mathbf{n}^-$ are unit vectors perpendicular to Γ pointing away from regions $+$ and $-$ respectively. The second equation in (2) implies that the gradient of the solution is not continuous across the interface Γ. Standard finite element methods use polynomial basis functions in the support of each elements, which are C^∞ functions. Therefore when an element crosses the interfaces Γ, the approximation of the solution is very poor since C^∞ functions struggle to approximate a solution that is not even C^1. Normally this limitation is resolved by aligning the edges of the elements in the mesh along with Γ. Since standard FEMs are supposed to be only C^0 across edges and faces, this helps to regain a good convergence speed. Therefore, in the presence of a meso-scale or a micro-scale, standard FEMs need very fine meshes to perform well.

3. Multi-region DGCFE method

To overcome the limitations of standard FEMs on problems with meso-scales or micro-scales, we propose to extend the DGCFE method in such a way that no element crosses Γ and Γ is always described by the edges of the elements. At the same time, the flexibility of the DGCFE method allows for elements much larger than the size of the regions $\mathcal{C}_j$.

The key idea of DGCFEM is to exploit general shaped elements upon which elemental basis functions may only be locally piecewise smooth. In particular, a Composite Finite Element (CFE) may be seen as an aggregation of standard elements, with the basis functions on the CFE being constructed as a linear combination of the basis functions defined on the standard elements used in the aggregation; see [4] for further details. In this way, a mesh composed of CFEs may describe very complex domains with a small number of elements. To accomplish this, two meshes are used in the DGCFE method. Borrowing the notation from [4], we denote with $\mathcal{T}_{\mathrm{CFE}}$ the coarse level mesh formed by CFEs, which is assumed to be too coarse for the problem in the standard FEM way and with $\mathcal{T}_{h_\ell}$ the fine level mesh of standard

5

elements that describes all the details in the domain and the boundaries of the regions $\mathcal{C}_j$. Each fine element in $\mathcal{T}_{h_\ell}$ is considered as a child of the coarse element in $\mathcal{T}_{\text{CFE}}$ that contains its centre. The easiest way to defines the two meshes $\mathcal{T}_{h_\ell}$ and $\mathcal{T}_{\text{CFE}}$ is to construct them independently using a standard mesh generator. In [4, Section 3] a different method to construct $\mathcal{T}_{h_\ell}$ and $\mathcal{T}_{\text{CFE}}$ is presented. In such method, the mesh $\mathcal{T}_{h_\ell}$ is derived from a coarse conforming mesh $\mathcal{T}_H$ by applying adaptive refinement. Then the mesh $\mathcal{T}_{\text{CFE}}$ is derived from $\mathcal{T}_H$ by restricting the support of the elements to the domain Ω. Such construction can be extended to cover the case considered in this paper. For the sake of brevity, we do not report the full algorithm here, we only indicate the differences from the algorithm in [4]. The initial mesh is assumed to be very coarse, so coarse that it is not even possible to describe the outer shape of the domain. In the algorithm in [4, Section 3] an element κ is refined if it is not fully contained in the physical domain Ω. To construct the fine mesh $\mathcal{T}_{h_\ell}$ for the case with discontinuous coefficients, it is necessary to refine also all elements κ that are not fully contained in only one of the regions $\mathcal{R}_i$. The maximum number of refinement steps used to construct $\mathcal{T}_{h_\ell}$ is set with the input parameters. The index ℓ in this case indicates the number of refinement levels between the coarse and the fine mesh. As in [4], in the final stage of the process of the construction of $\mathcal{T}_{h_\ell}$ the nodes may be moved in the same way as explained in [4], not only to fit better $\partial\Omega$, but also the boundaries $\partial\mathcal{R}_i$ of the regions. The displacement of the nodes can be seen as the action of a bijective mapping ϕ. In this way, the fine mesh is constructed in such a way to describe the different regions $\mathcal{R}_i$.

Remark 3.1. *To make the presentation of the method easier, we assume in this paper that the domain Ω has a simple shape. In this way, we can focus on the small scale structure formed by the regions where $\mathcal{A}$ assumes different values. Therefore we assume that the element $\kappa_{\text{CFE}} \in \mathcal{T}_{\text{CFE}}$ is a standard looking element. Domains with complicated shapes are not a difficulty for the MRDGCFEM since the method is based on DGCFE which is specifically designed for the task.*

The methods presented so far to construct $\mathcal{T}_{\text{CFE}}$ do not guarantee that all coarse elements $\kappa_{\text{CFE}} \in \mathcal{T}_{\text{CFE}}$ are all contained in only one region $\mathcal{R}_i$. In general, it is just the opposite since we want the sizes of the elements κ_{CFE} to be bigger than the sizes of the regions $\mathcal{R}_i$. In this way, the number of κ_{CFE} elements may not be linked to the number and sizes of the regions $\mathcal{C}_i$.
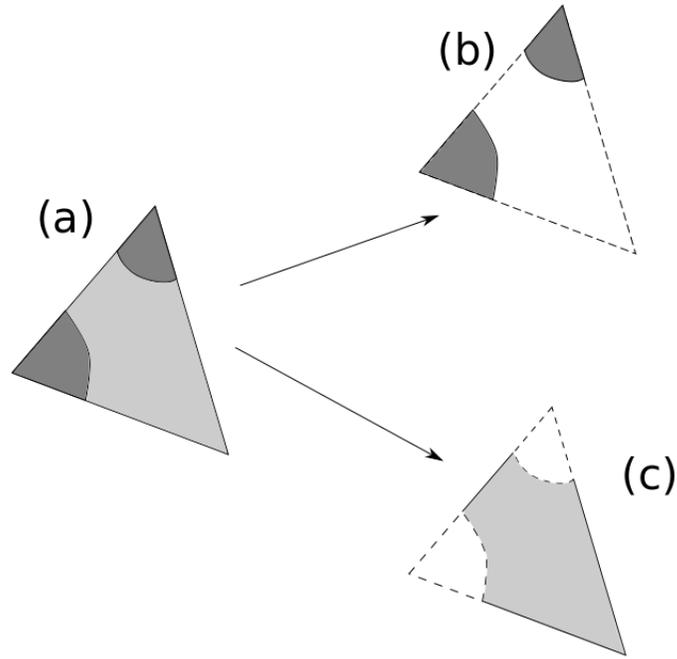
Figure 1: Decomposition of a composite element (a) intersecting two regions $\mathcal{R}_i$ into two $\kappa_{\mathrm{CFE},i}$ multi-region elements (b-c). The element in (a) intersects two different regions indicated in dark and light gray. The multi-region element in (b) is the intersection between the element and the first region. Similarly, the multi-region element in (c) is the intersection between the element and the second region.

Hence, we define $\kappa_{\mathrm{CFE},i} := \kappa_{\mathrm{CFE}} \cap \mathcal{R}_i \neq \emptyset$, where κ_{CFE} is any coarse level element and $\mathcal{R}_i$ is any of the regions, see Figure 1 for a representation of such operation. All elements κ_{CFE} intersect at least one region $\mathcal{R}_i$, i.e. for any element κ_{CFE} there is at least a region $\mathcal{R}_i$ such that $\kappa_{\mathrm{CFE},i} \neq \emptyset$. In general, we assume that each element κ_{CFE} may intersect more than one region $\mathcal{R}_i$, i.e. for a given element κ_{CFE}, $\kappa_{\mathrm{CFE},i} \neq \emptyset$ for more than one value for i. Also, it is safe to assume in most cases that $\kappa_{\mathrm{CFE},i}$ may be a disconnected region. Contrarily, each element $\kappa \in \mathcal{T}_{h_\ell}$ is contained by construction in only one region $\mathcal{R}_i$, for some i.

To extend the DGCFE method to problems with discontinuous coefficients, we need to define a different coarse level mesh. Let define $\mathcal{T}_{\mathrm{CFE}}^{\mathrm{disc}}$ the composite finite element mesh consisting of all composite elements $\kappa_{\mathrm{CFE},i} \neq \emptyset$ for any combination of κ_{CFE} and $\mathcal{R}_i$. For simplicity we indicate the element of $\mathcal{T}_{\mathrm{CFE}}^{\mathrm{disc}}$ with $\kappa_{\mathrm{CFE}}^{\mathrm{disc}}$. From the definition is straightforward to see that $\mathcal{T}_{\mathrm{CFE}} \subseteq \mathcal{T}_{\mathrm{CFE}}^{\mathrm{disc}} \subseteq \mathcal{T}_{h_\ell}$ meaning that all elements of $\mathcal{T}_{\mathrm{CFE}}^{\mathrm{disc}}$ can be seen as aggregations of elements in $\mathcal{T}_{h_\ell}$. The elements $\kappa \in \mathcal{T}_{h_\ell}$ forming an element $\kappa_{\mathrm{CFE}}^{\mathrm{disc}}$ are called its children and indicated with the set $\mathcal{S}(\kappa_{\mathrm{CFE}}^{\mathrm{disc}}) \subseteq \mathcal{T}_{h_\ell}$.

Defining a vector of positive integers $\mathbf{p}$ of the same length as the number of elements in $\mathcal{T}_{h_\ell}$, the DG finite element space on $\mathcal{T}_{h_\ell}$ is defined in the standard way as in [4]:

$$V(\mathcal{T}_{h_\ell}, \mathbf{p}) = \{u \in L_2(\Omega) : u|_\kappa \in \mathcal{P}_{p_\kappa}(\kappa) \ \forall \kappa \in \mathcal{T}_{h_\ell}\},$$

where the polynomial space $\mathcal{P}_{p_\kappa}(\kappa)$ could coincide with either $\mathbb{Q}_{p_\kappa}(\kappa)$ or $\mathbb{P}_{p_\kappa}(\kappa)$ depending on the problem to solve and p_κ is the entry in $\mathbf{p}$ corresponding to the element κ. The construction of the finite element space $V(\mathcal{T}_{\mathrm{CFE}}^{\mathrm{disc}}, \mathbf{p})$ on $\mathcal{T}_{\mathrm{CFE}}^{\mathrm{disc}}$ is inspired to the finite element space constructed on $\mathcal{T}_{\mathrm{CFE}}$ in [4]. On each coarse element $\kappa_{\mathrm{CFE}}^{\mathrm{disc}}$ we define a polynomial space $\mathcal{P}_{p_{\kappa_{\mathrm{CFE}}^{\mathrm{disc}}}}(\kappa_{\mathrm{CFE}}^{\mathrm{disc}})$ which should satisfy the condition: For any $\kappa_{\mathrm{CFE}}^{\mathrm{disc}} \in \mathcal{T}_{\mathrm{CFE}}^{\mathrm{disc}}$ we have that for any $\kappa \in \mathcal{S}(\kappa_{\mathrm{CFE}}^{\mathrm{disc}})$ holds

$$\mathcal{P}_{p_{\kappa_{\mathrm{CFE}}^{\mathrm{disc}}}}(\kappa_{\mathrm{CFE}}^{\mathrm{disc}})|_{\mathrm{supp}(\kappa)} \subseteq \mathcal{P}_{p_\kappa}(\kappa) \ , \tag{3}$$

or in other words the restriction of the space $\mathcal{P}_{p_{\kappa_{\mathrm{CFE}}^{\mathrm{disc}}}}(\kappa_{\mathrm{CFE}}^{\mathrm{disc}})$ to the support of any of the children elements is contained in the polynomial space of the child element. The condition (3) guarantees that any basis function living on the coarse elements can be described as a linear combination of basis functions living on the fine level elements. Denoting the coarse level basis function

with $\phi_{\texttt{CFE},i}$, with $i = 1, \ldots, \dim(V(\mathcal{T}_{\text{CFE}}^{\text{disc}}, \mathbf{p}))$ and denoting the fine level basis functions with $\phi_{h_\ell,j}$, with $j = 1, \ldots, \dim(V(\mathcal{T}_{h_\ell}, \mathbf{p}))$, we have that there are real coefficients $\alpha_{i,j}$ such that

$$\phi_{\texttt{CFE},i} := \sum_{j=1,\ldots,\dim(V(\mathcal{T}_{h_\ell},p))} \alpha_{i,j} \phi_{h_\ell,j} \ . \tag{4}$$

This construction is equivalent to define on each coarse element $\kappa_{\text{CFE}}^{\text{disc}}$ a standard polynomial space restricted to the support of $\kappa_{\text{CFE}}^{\text{disc}}$. In view of this, the fact that the elements $\kappa_{\text{CFE}}^{\text{disc}}$ may be disconnected is not an issue, as this is not an issue for the DGCFE method either.

In order to define the MRDGCFE method on $\mathcal{T}_{\text{CFE}}^{\text{disc}}$, we denote by $\mathcal{F}_{\texttt{disc}}^{\mathcal{I}}$ the set of all interior faces of the partition $\mathcal{T}_{\text{CFE}}^{\text{disc}}$ of Ω, and by $\mathcal{F}_{\texttt{disc}}^{\mathcal{B}}$ the set of all boundary faces of $\mathcal{T}_{\text{CFE}}^{\text{disc}}$. Furthermore, we define $\mathcal{F}_{\texttt{disc}} = \mathcal{F}_{\texttt{disc}}^{\mathcal{I}} \cup \mathcal{F}_{\texttt{disc}}^{\mathcal{B}}$. It is important to notice that the elements in $\mathcal{T}_{\text{CFE}}^{\text{disc}}$ are not standard elements so their number of faces may vary significantly from element to element. However, any face in the mesh $\mathcal{T}_{\text{CFE}}^{\text{disc}}$ can be seen as an aggregation of faces of $\mathcal{T}_{h_\ell}$. Let $(\kappa_{\text{CFE}}^{\text{disc}})^+$ and $(\kappa_{\text{CFE}}^{\text{disc}})^-$ be two adjacent elements of $\mathcal{T}_{\text{CFE}}^{\text{disc}}$, and $\mathbf{x}$ an arbitrary point on the interior face $F \in \mathcal{F}_{\texttt{disc}}^{\mathcal{I}}$ given by $F = \partial(\kappa_{\text{CFE}}^{\text{disc}})^+ \cap \partial(\kappa_{\text{CFE}}^{\text{disc}})^-$. Let also v and $\mathbf{q}$ be scalar- and vector-valued functions, respectively, that are smooth inside each element $(\kappa_{\text{CFE}}^{\text{disc}})^\pm$. We denote with $(v^\pm, \mathbf{q}^\pm)$ the traces of $(v, \mathbf{q})$ on F taken from within the interior of $(\kappa_{\text{CFE}}^{\text{disc}})^\pm$, respectively. We also define the average $\mathbf{q}$ at $\mathbf{x} \in F$ as

$$\{\!\!\{\mathbf{q}\}\!\!\} = \frac{1}{2}(\mathbf{q}^+ + \mathbf{q}^-).$$

Similarly, we define the jump of v at $\mathbf{x} \in F$ as

$$[\![v]\!] = v^+ \mathbf{n}_{(\kappa_{\text{CFE}}^{\text{disc}})}^+ + v^- \mathbf{n}_{(\kappa_{\text{CFE}}^{\text{disc}})}^-,$$

where we denote by $\mathbf{n}_{(\kappa_{\text{CFE}}^{\text{disc}})}^\pm$ the unit outward normal vector of $\partial(\kappa_{\text{CFE}}^{\text{disc}})^\pm$, respectively. On a boundary face $F \in \mathcal{F}_{\texttt{disc}}^{\mathcal{B}}$ the definition of the average and jump are $\{\!\!\{\mathbf{q}\}\!\!\} = \mathbf{q}$ and $[\![v]\!] = v\mathbf{n}$, with $\mathbf{n}$ denoting the unit outward normal vector on the boundary $\partial\Omega$. We also assume that the assumptions (A1), (A2) and (A3) in [4] are satisfied.

With this notation, we define the weak MRDGCFE formulation for the numerical approximation of problem (1) as find $u_h \in V(\mathcal{T}_{\text{CFE}}^{\text{disc}}, \mathbf{p})$ such that

$$B_{\texttt{DG}}(u_h, v) = F_h(v) \tag{5}$$

9

for all $v \in V(\mathcal{T}_{\text{CFE}}^{\text{disc}}, \mathbf{p})$, where

$$B_{\text{DG}}(u, v) = \sum_{\kappa \in \mathcal{T}_{\text{CFE}}^{\text{disc}}} \int_{\kappa} \mathcal{A}\nabla u \cdot \nabla v \, d\mathbf{x} - \sum_{F \in \mathcal{F}_{\text{disc}}^{\mathcal{I}} \cup \mathcal{F}_{\text{disc}}^{\mathcal{B}}} \int_F \left(\{\!\{\mathcal{A}\nabla v\}\!\} \cdot [\![u]\!] + \{\!\{\mathcal{A}\nabla u\}\!\} \cdot [\![v]\!] \right) ds$$

$$+ \sum_{F \in \mathcal{F}_{\text{disc}}^{\mathcal{I}} \cup \mathcal{F}_{\text{disc}}^{\mathcal{B}}} \int_F \sigma \, [\![u]\!] \cdot [\![v]\!] \, ds,$$

$$F_h(v) = \int_{\Omega} fv \, d\mathbf{x} - \sum_{F \in \mathcal{F}_{\text{disc}}^{\mathcal{B}}} \int_F \mathcal{A}\nabla v \cdot \mathbf{n}_F g \, ds + \sum_{F \in \mathcal{F}_{\text{disc}}^{\mathcal{B}}} \int_F \sigma \, gv \, ds,$$

where $\mathbf{n}_F$ is the unit outward normal vector of F and where the function $\sigma \in L^{\infty}(\mathcal{F}_{\text{disc}})$ is the discontinuity stabilization function that is chosen as follows

$$\sigma|_F = \gamma \mathcal{A}_F p_F^2 h_F^{-1}, \tag{6}$$

where on interior faces p_F is the maximum of the order of the elements sharing F and on boundary edges p_F is the order of the element containing F. Similarly, on interior faces $\mathcal{A}_F$ is the maximum value of $\mathcal{A}$ among the two elements sharing the face F and on boundary edges $\mathcal{A}_F$ is the value of $\mathcal{A}$ of the element containing F. The parameter $\gamma > 0$ is independent of h_F and p_F.

In the weak formulation (5), the discontinuous coefficient $\mathcal{A}$ is incorporated in flux terms and in the penalty term in the most simple way possible. The value of $\mathcal{A}$ is used to adjust the penalisation on faces to compensate for the difference in the diffusion coefficients in different parts of the domain. Such modification of the DG method works well when the jumps in the values of $\mathcal{A}$ are not too extreme. A more robust way to treat discontinuous diffusion coefficients can be found in [13].

3.1. A priori convergence

The a priori convergence analysis for the MRDGCFE method is an extension of the analysis in [4] to take into account the partition of the CFEs in different regions. The extension in this case is simple because the DGCFE method in [4] can handle CFEs of any shape and the elements $\kappa_{\text{CFE}}^{\text{disc}}$ can be seen as CFEs of various shapes. As in [4], the a priori convergence result makes use of the following extension result from [26, Theorem 5, p. 181]:

Theorem 3.2. *Let Ω be a domain with a Lipschitz boundary. Then there exists a linear extension operator $\mathfrak{E} : H^s(\Omega) \to H^s(\mathbb{R}^d)$, $s \in \mathbb{N}_0$, such that $\mathfrak{E}v|_\Omega = v$ and*

$$\|\mathfrak{E}v\|_{H^s(\mathbb{R}^d)} \leq C\|v\|_{H^s(\Omega)},$$

where C is a positive constant depending only on s and Ω.

As in [4], the a priori result is restricted to problems with solutions with local regularity at least in H^2. This is the case for the problems presented in Section 5.1 and in Section 5.2. In general, problems with non-smooth interfaces between the different regions $\mathcal{R}_i$ have weaker regularity. The regularity assumption may be weakened as suggested in Remark 7.4 in [4].

Defining the DG norm as

$$||| v |||^2_{\text{DG}} = \sum_{\kappa \in \mathcal{T}^{\text{disc}}_{\text{CFE}}} \|\mathcal{A}^{\frac{1}{2}}\nabla v\|^2_{L_2(\kappa)} + \sum_{F \in \mathcal{F}_{\text{disc}}} \|\sigma^{\frac{1}{2}}[\![v]\!]\|^2_{L_2(F)}, \tag{7}$$

the following results proves that the DG norm of the error can be bounded by the norm of the solution to the problem.

Theorem 3.3. *Let $\Omega \in \mathbb{R}^d$ be a bounded polyhedral domain, and let $\mathcal{T}^{\text{disc}}_{\text{CFE}}$ be a subdivision of Ω as described above. Let $u_h \in V(\mathcal{T}^{\text{disc}}_{\text{CFE}}, \mathbf{p})$ be the MRDGCFE approximation to u defined by (5). Assuming that the local regularity of u in each $\kappa \in \mathcal{T}^{\text{disc}}_{\text{CFE}}$ is such that $u|_\kappa \in H^{K_\kappa}(\kappa)$ for integers $K_\kappa \geq 2$. Then the following error bound holds with a constant C independent of the size and order of the elements in $\mathcal{T}^{\text{disc}}_{\text{CFE}}$ and the variations of $\mathcal{A}$:*

$$||| u - u_h |||^2_{\text{DG}} \leq \mathcal{A}_{\max} C \sum_{\kappa \in \mathcal{T}^{\text{disc}}_{\text{CFE}}} \frac{h_\kappa^{2s_\kappa}}{h_F^2} \frac{1}{2p_\kappa^{2K_\kappa - 3}} \|\mathfrak{E}\tilde{u}\|^2_{H_{K_\kappa}(\kappa_{\text{CFE}})} \ ,$$

for any integers s_κ, $1 \leq s_\kappa \leq \min(p_\kappa + 1, K_\kappa)$ with $p_\kappa \geq 1$ and where h_κ is the diameter of κ. Moreover, we denote by κ_{CFE} the CFE in $\mathcal{T}_{\text{CFE}}$ for which there is region $\mathcal{R}_i$ such that $\kappa = \kappa_{\text{CFE}} \cap \mathcal{R}_i$ and we define $\tilde{u} := u \circ \phi$.

The proof of Theorem 3.3 follows the same argument as the proof of Theorem 7.2 in [4].

Remark 3.4. *Theorem 3.3 holds under the assumption in Remark 3.1. In case that the shape of the domain Ω is complicated, the result in Theorem 3.3*

11

would be:

$$||| \, u - u_h \, |||^2_{\mathrm{DG}} \leq \mathcal{A}_{\mathrm{max}} C \sum_{\kappa \in \mathcal{T}^{\mathrm{disc}}_{\mathrm{CFE}}} \frac{h_\kappa^{2s_\kappa}}{h_F^2} \frac{1}{2p_\kappa^{2K_\kappa - 3}} \| \mathfrak{E} \tilde{u} \|^2_{H_{K_\kappa}(\hat{\kappa})} \ ,$$

where $\hat{\kappa}$ is the element of the coarse mesh $\mathcal{T}_H$ that contains κ, see [4] for more details.

4. A posteriori error estimator

In this section, we present the a posteriori error estimator η to drive the adaptivity for the MRDGCFE method:

$$\eta := \left(\sum_{\kappa \in \mathcal{T}^{\mathrm{disc}}_{\mathrm{CFE}}} \eta_\kappa^2 \right)^{\frac{1}{2}} , \tag{8}$$

where the terms η_κ in (8) are defined as:

$$
\begin{aligned}
\eta_\kappa^2 \ = \ & h_\kappa^2 p_\kappa^{-2} \| \Pi f + \nabla \cdot (\mathcal{A} \nabla u_h) \|^2_{L_2(\kappa)} \\
& + \sum_{F \subset \mathcal{F}^{\mathcal{I}}_{\mathrm{disc}}(\kappa)} h_\kappa^2 h_F^{-1} p_\kappa^{-1} \| [\![\mathcal{A} \nabla u_h]\!] \|^2_{L_2(F)} + \sum_{F \subset \mathcal{F}^{\mathcal{I}}_{\mathrm{disc}}(\kappa)} \sigma h_\kappa^2 h_F^{-2} p_\kappa \| [\![u_h]\!] \|^2_{L_2(F)} \tag{9} \\
& + \sum_{F \subset \mathcal{F}^{\mathcal{B}}_{\mathrm{disc}}(\kappa)} \sigma h_\kappa^2 h_F^{-2} p_\kappa \| u_h - \Pi g \|^2_{L_2(F)}, \tag{10}
\end{aligned}
$$

where $\mathcal{F}^{\mathcal{I}}_{\mathrm{disc}}(\kappa)$ and $\mathcal{F}^{\mathcal{B}}_{\mathrm{disc}}(\kappa)$ are respectively $\mathcal{F}^{\mathcal{I}}_{\mathrm{disc}} \cap \partial \kappa$ and $\mathcal{F}^{\mathcal{B}}_{\mathrm{disc}} \cap \partial \kappa$ and where we denote by Π the L_2–projection onto $V(\mathcal{T}^{\mathrm{disc}}_{\mathrm{CFE}}, \mathtt{p})$. The error estimator η is the adaptation of the error estimator presented in [17] to the current case with multiple regions $\mathcal{R}_i$.

Remark 4.1. *Slightly modifying the argument in [17], it is possible to prove the reliability of the error estimator η, i.e.*

$$||| \, u - u_h \, |||_{\mathrm{DG}} \leq C \left(\sum_{\kappa \in \mathcal{T}^{\mathrm{disc}}_{\mathrm{CFE}}} (\eta_\kappa^2 + \mathcal{O}_\kappa^2) \right)^{\frac{1}{2}} ,$$

with a constant C independent of the size or order of the elements in $\mathcal{T}^{\mathrm{disc}}_{\mathrm{CFE}}$ and with

$$\mathcal{O}_\kappa := \left(h_\kappa^2 p_\kappa^{-2} \| f - \Pi f \|^2_{L_2(\kappa)} + \sum_{F \in \mathcal{F}^{\mathcal{B}}_{\mathrm{disc}}(\kappa)} \sigma h_\kappa^2 h_F^{-2} p_F \| g - \Pi g \|^2_{L_2(F)} \right)^{\frac{1}{2}} .$$

12

5. Numerics

In this section, we present a series of computational examples to highlight the performances of the MRDGCFE method for problems where the underlying computational domain contains inclusions. Throughout this section the MRDGCFE solution u_h in (5) is computed with the constant γ appearing in the discontinuity stabilization function σ equal to 10.

Algorithm 5.1 Adaptive Refinement Algorithm

1: Input parameters: refinement fraction θ_r; termination tolerance tol; maximum number of refinement steps $n_{\mathtt{max}}$; type of adaptive refinement.
2: Initial step: Input initial composite finite element mesh $\mathcal{T}_{\mathrm{CFE}}^{\mathrm{disc}}$ and fine level mesh $\mathcal{T}_{h_\ell}$ and and the corresponding finite element spaces $V(\mathcal{T}_{\mathrm{CFE}}^{\mathrm{disc}}, \mathbf{p})$ and $V(\mathcal{T}_{h_\ell}, \mathbf{p})$.
3: Set $n = 1$.
4: **while** $n < n_{\mathtt{max}}$ **do**
5:     Compute $u_h \in V(\mathcal{T}_{\mathrm{CFE}}^{\mathrm{disc}}, \mathbf{p})$ solving (5).
6:     Evaluate the error indicators η_κ, defined by (10), for all $\kappa \in \mathcal{T}_{\mathrm{CFE}}^{\mathrm{disc}}$
7:     **if** $\eta < \mathrm{tol}$ **then**
8:         Exit.
9:     **else**
10:         Mark elements for refinement employing the fixed fraction refinement strategy with refinement fraction θ_r.
11:         **if** Element κ is marked for refinement **then**
12:             Depending on what type of adaptive refinement between h and p has been requested, the marked elements are marked for the requested refinement.
13:         **end if**
14:         Set $n = n + 1$ and adaptively refine the finite element space $V(\mathcal{T}_{\mathrm{CFE}}^{\mathrm{disc}}, \mathbf{p})$ and the mesh $\mathcal{T}_{\mathrm{CFE}}^{\mathrm{disc}}$.
15:         Refine the fine level finite element space $V(\mathcal{T}_{h_\ell}, \mathbf{p})$ and the mesh $\mathcal{T}_{h_\ell}$ (if necessary), to ensure that the inclusion $V(\mathcal{T}_{\mathrm{CFE}}^{\mathrm{disc}}, \mathbf{p}) \subseteq V(\mathcal{T}_{h_\ell}, \mathbf{p})$ holds.
16:     **end if**
17: **end while**

Algorithm 5.1 outlines the general adaptive algorithm employed in this section. The last step of Algorithm 5.1 ensures the compatibility condition

$V(\mathcal{T}_{\mathrm{CFE}}^{\mathrm{disc}}, \mathtt{p}) \subseteq V(\mathcal{T}_{h_\ell}, \mathtt{p})$ which is fundamental for the MRDGCFE method since such condition is exploited in the construction of the coarse level shape functions, cf. (4).

In this section, the MRDGCFE method is compared against the DGCFE method. The DGCFE method is the discontinuous Galerkin composite finite element method presented in [4]. The difference between the MRDGCFE method and the DGCFE method is that the composite finite elements in the DGCFE method may not respect the subdivision $\mathcal{C}_j$ of the domain Ω. The DGCFE method is designed for problems with complicated domains and not for problems with discontinuous coefficients. In general, it may happen that a composite finite element in the DGCFE method intersects more than one region $\mathcal{R}_i$. Using $V(\mathcal{T}_{\mathrm{CFE}}, \mathbf{p})$ to indicate the finite element space for the DGCFE method introduced in [4], we have that the variational formulation for the DGCFE method of problem (1) is:

$$B_{\mathtt{DG}}^{\mathtt{DGCFE}}(u_h, v) = F_h^{\mathtt{DGCFE}}(v)$$

for all $v \in V(\mathcal{T}_{\mathrm{CFE}}, \mathbf{p})$, where

$$B_{\mathtt{DG}}^{\mathtt{DGCFE}}(u, v) = \sum_{\kappa \in \mathcal{T}_{\mathrm{CFE}}} \int_\kappa \mathcal{A}\nabla u \cdot \nabla v \, d\mathbf{x} - \sum_{F \in \mathcal{F}^\mathcal{I} \cup \mathcal{F}^\mathcal{B}} \int_F \left(\{\!\{\mathcal{A}\nabla v\}\!\} \cdot [\![u]\!] + \{\!\{\mathcal{A}\nabla u\}\!\} \cdot [\![v]\!] \right) ds$$
$$+ \sum_{F \in \mathcal{F}^\mathcal{I} \cup \mathcal{F}^\mathcal{B}} \int_F \sigma \, [\![u]\!] \cdot [\![v]\!] \, ds,$$
$$F_h^{\mathtt{DGCFE}}(v) = \int_\Omega f v \, d\mathbf{x} - \sum_{F \in \mathcal{F}^\mathcal{B}} \int_F \mathcal{A}\nabla v \cdot \mathbf{n}_F g \, ds + \sum_{F \in \mathcal{F}^\mathcal{B}} \int_F \sigma \, g v \, ds,$$

where $\mathcal{F}^\mathcal{I}$ and $\mathcal{F}^\mathcal{B}$ are respectively the set of all interior faces and the set of all boundary faces of $\mathcal{T}_{\mathrm{CFE}}$. The DG norm for the DGCFE method is defined as:

$$||\!|\, v \,|\!||_{\mathtt{DG}}^2 = \sum_{\kappa \in \mathcal{T}_{\mathrm{CFE}}} \|\mathcal{A}^{\frac{1}{2}}\nabla v\|_{L_2(\kappa)}^2 + \sum_{F \in \mathcal{F}^\mathcal{I} \cup \mathcal{F}^\mathcal{B}} \|\sigma^{\frac{1}{2}}[\![v]\!]\|_{L_2(F)}^2.$$

For the DGCFE method, the a posteriori error estimator for problem (1) is defined as:

$$\eta := \left(\sum_{\kappa \in \mathcal{T}_{\mathrm{CFE}}} \eta_\kappa^2 \right)^{\frac{1}{2}},$$

14

where

$$
\begin{aligned}
\eta_\kappa^2 \;=\;& h_\kappa^2 p_\kappa^{-2}\|\Pi f + \nabla\cdot(\mathcal{A}\nabla u_h)\|_{L_2(\kappa)}^2 \\
&+ \sum_{F\subset\mathcal{F}^\mathcal{I}(\kappa)} h_\kappa^2 h_F^{-1} p_\kappa^{-1}\|[\![\mathcal{A}\nabla u_h]\!]\|_{L_2(F)}^2 + \sum_{F\subset\mathcal{F}^\mathcal{I}(\kappa)} \sigma h_\kappa^2 h_F^{-2} p_\kappa\|[\![u_h]\!]\|_{L_2(F)}^2 \\
&+ \sum_{F\subset\mathcal{F}^\mathcal{B}(\kappa)} \sigma h_\kappa^2 h_F^{-2} p_\kappa\|u_h - \Pi g\|_{L_2(F)}^2,
\end{aligned}
$$

where $\mathcal{F}^\mathcal{I}(\kappa)$ and $\mathcal{F}^\mathcal{B}(\kappa)$ are respectively $\mathcal{F}^\mathcal{I}\cap\partial\kappa$ and $\mathcal{F}^\mathcal{B}\cap\partial\kappa$ and where we denote by Π the L_2–projection onto $V(\mathcal{T}_{\text{CFE}},\mathtt{p})$.

Also, in this section, the SIPDG method is mentioned. The SIPDG method is the symmetric interior penalty discontinuous Galerkin method [5] applied to (1). The variational formulation for the SIPDG method for problem (1) is:

$$
B_{\text{DG}}^{\text{SIPDG}}(u_h,v) = F_h^{\text{SIPDG}}(v)
$$

for all $v \in V(\mathcal{T}_H,\mathbf{p})$, where

$$
B_{\text{DG}}^{\text{SIPDG}}(u,v) = \sum_{\kappa\in\mathcal{T}_H}\int_\kappa \mathcal{A}\nabla u\cdot\nabla v\,d\mathbf{x} - \sum_{F\in\mathcal{F}_{\text{SIPDG}}^\mathcal{I}\cup\mathcal{F}_{\text{SIPDG}}^\mathcal{B}}\int_F \left(\{\!\{\mathcal{A}\nabla v\}\!\}\cdot[\![u]\!] + \{\!\{\mathcal{A}\nabla u\}\!\}\cdot[\![v]\!]\right)ds
$$

$$
+ \sum_{F\in\mathcal{F}_{\text{SIPDG}}^\mathcal{I}\cup\mathcal{F}_{\text{SIPDG}}^\mathcal{B}}\int_F \sigma\,[\![u]\!]\cdot[\![v]\!]\,ds,
$$

$$
F_h^{\text{SIPDG}}(v) = \int_\Omega fv\,d\mathbf{x} - \sum_{F\in\mathcal{F}_{\text{SIPDG}}^\mathcal{B}}\int_F \mathcal{A}\nabla v\cdot\mathbf{n}_F g\,ds + \sum_{F\in\mathcal{F}_{\text{SIPDG}}^\mathcal{B}}\int_F \sigma\,gv\,ds,
$$

where $\mathcal{F}_{\text{SIPDG}}^\mathcal{I}$ and $\mathcal{F}_{\text{SIPDG}}^\mathcal{B}$ are respectively the set of all interior faces and the set of all boundary faces of $\mathcal{T}_H$. Moreover, the DG norm for the SIPDG method is defined as:

$$
|\!|\!| v |\!|\!|_{\text{DG}}^2 = \sum_{\kappa\in\mathcal{T}_H}\|\mathcal{A}^{\frac{1}{2}}\nabla v\|_{L_2(\kappa)}^2 + \sum_{F\in\mathcal{F}_{\text{SIPDG}}^\mathcal{I}\cup\mathcal{F}_{\text{SIPDG}}^\mathcal{B}}\|\sigma^{\frac{1}{2}}[\![v]\!]\|_{L_2(F)}^2.
$$

5.1. Convergence study

In this section, we explore the convergence of the MRDGCFE method. We are particularly interested in showing the ability of MRDGCFEs to achieve good approximation in the cases where the coarse mesh is too coarse

15

to describe the regions $\mathcal{R}_i$. The comparison is done between the MRDGCFE and the DGCFE method. To do the comparison, a non-smooth problem on the domain $\Omega = [0,1]^2$ with a known analytical solution is used. The prescribed solution is not regular across the segment $x_0 \times [0,1]$, for x_0 to be specified later. The problem is defined as

$$
\begin{aligned}
-\nabla \cdot (\mathcal{A}\nabla u) &= f \quad \text{in } \Omega , \\
u &= g \quad \text{on } \partial\Omega ,
\end{aligned}
\tag{11}
$$

where $\mathcal{A} = 1$ in $[0, x_0] \times [0,1]$ and $\mathcal{A} = 100$ in $(x_0, 1] \times [0,1]$ and $f(x,y)$ and $g(x,y)$ are derived from the solution $u(x,y)$. In the region $[0, x_0] \times [0,1]$ the solution $u(x,y)$ is defined as $\sin(\pi x)$; while in the region $(x_0, 1] \times [0,1]$, $u(x,y)$ is defined as $\alpha x + \beta$ where the values of α and β are such that the continuity of the solution along $x_0 \times [0,1]$ is ensured and the jumping condition across $x_0 \times [0,1]$ is satisfied, i.e.

$$
\begin{aligned}
\lim_{x \to x_0^-} u - \lim_{x \to x_0^+} u &= 0, \quad \forall y \in [0,1], \\
\lim_{x \to x_0^-} \left(A\nabla u \cdot \mathbf{n}^-\right) + \lim_{x \to x_0^+} \left(A\nabla u \cdot \mathbf{n}^+\right) &= 0, \quad \forall y \in [0,1],
\end{aligned}
\tag{12}
$$

where $\mathbf{n}^- = (1,0)^T$ and $\mathbf{n}^+ = (-1,0)^T$.

Three values for x_0 are considered: 3/4, 11/16 and 45/64. Starting from a structured mesh of 2×2 square elements and doing multiple uniform h-refinements, the segments $x_0 \times [0,1]$ for such values of x_0 can be described by the edges of the adapted mesh after respectively 1, 3 and 5 uniform h-refinements. In other words, the segments $x_0 \times [0,1]$, for the prescribed values of x_0, are described by structured meshes of respectively 4×4, 16×16 and 64×64 elements. Any mesh coarser than those is not able to describe correctly the piecewise regions of coefficient $\mathcal{A}$.

In all the simulations the fine mesh $\mathcal{T}_{h_\ell}$ is a structured mesh of 64×64 square elements, which is the least fine mesh needed to describe well the interface for all considered positions of x_0. This implies that on the fine mesh the piecewise regions of coefficient $\mathcal{A}$ are always well described. For the coarse level composite meshes $\mathcal{T}_{\text{CFE}}$ we consider structured meshes with the following number of elements: 2×2, 4×4, 8×8, 16×16, 32×32 and 64×64 which may not describe well the regions $\mathcal{R}_i$. For the MRDGCFE method, the meshes $\mathcal{T}_{\text{CFE}}^{\text{disc}}$ are constructed as described in Section 3 starting from the $\mathcal{T}_{\text{CFE}}$ meshes. On all meshes, we use linear elements.

In Figure 2 the convergence of the L^2 and the DG norms of the error are reported for the two methods for the problem with $x_0 = 3/4$. Such

16
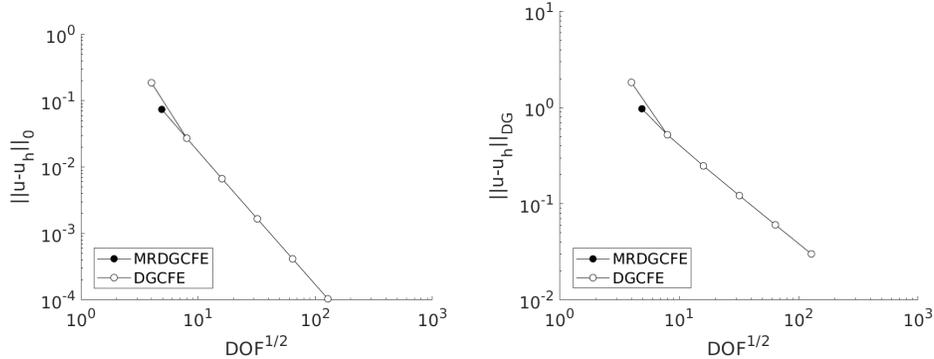
Figure 2: Results for the problem with $x_0 = 3/4$. (left) L^2 norm of the error. (right) DG norm of the error.

value of x_0 means that from the second coarser mesh onwards, the coarse mesh of both methods is fine enough to resolve the piecewise regions of coefficient $\mathcal{A}$, therefore the two methods are indistinguishable. But on the first mesh, the coarse mesh of both methods is too coarse to resolve the piecewise regions of coefficient $\mathcal{A}$. In such conditions, the DGCFE method delivers an approximation not in line with the rest of the plot. Instead, the MRDGCFE method delivers an approximation in line with the rest of the plot because the piecewise regions of the coefficient are captured on the coarse level mesh even if the mesh itself is not fine enough.

In Figure 3 the convergence of the L^2 and the DG norms of the error are reported for the two methods for the problem with $x_0 = 11/16$. In this case, only on the fourth mesh the coarse mesh of both methods is fine enough to capture the piecewise regions of the coefficient. The MRDGCFE method delivers consistent approximations on all meshes, while the DGCFE only on the fourth mesh onwards.

In Figure 4 the convergence of the L^2 and the DG norms of the error are reported for the two methods for the problem with $x_0 = 45/64$. In this case, only on the last mesh the coarse mesh of both methods is fine enough to capture the piecewise regions of the coefficient. While the DGCFE methods deliver not reliable approximations on all meshes except the last, the MRDGCFE shows a steady convergence.

Next, we solve again the same problems with x_0 equal to 3/4, 11/16 and 45/64 but this time increasing p uniformly on a sequence of meshes. The

17
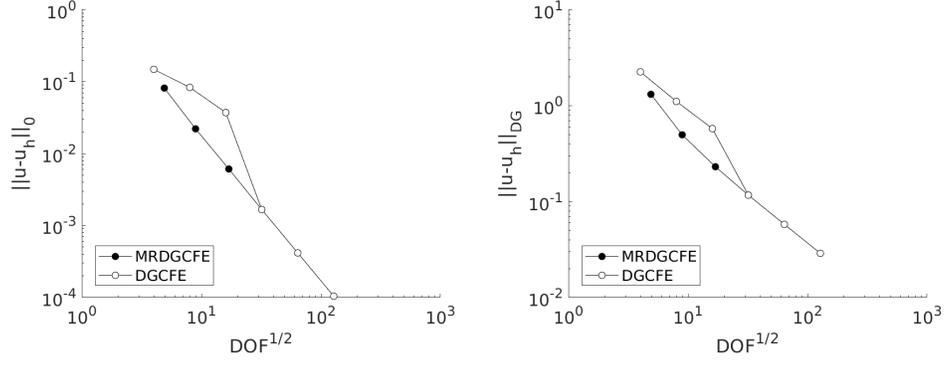
Figure 3: Results for the problem with $x_0 = 11/16$. (left) L^2 norm of the error. (right) DG norm of the error.
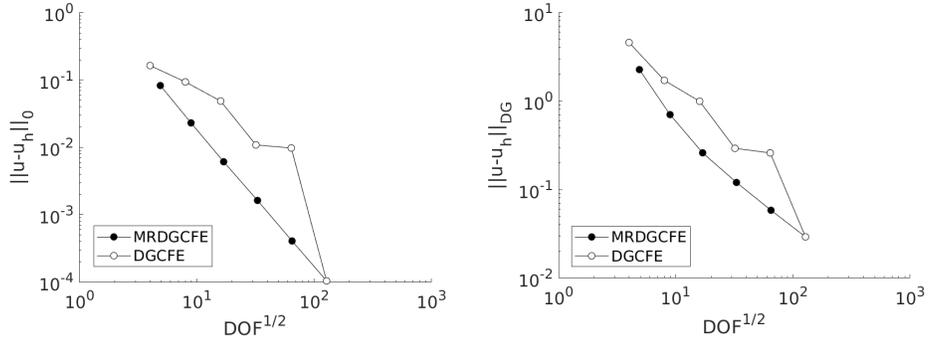
Figure 4: Results for the problem with $x_0 = 45/64$. (left) L^2 norm of the error. (right) DG norm of the error.

18
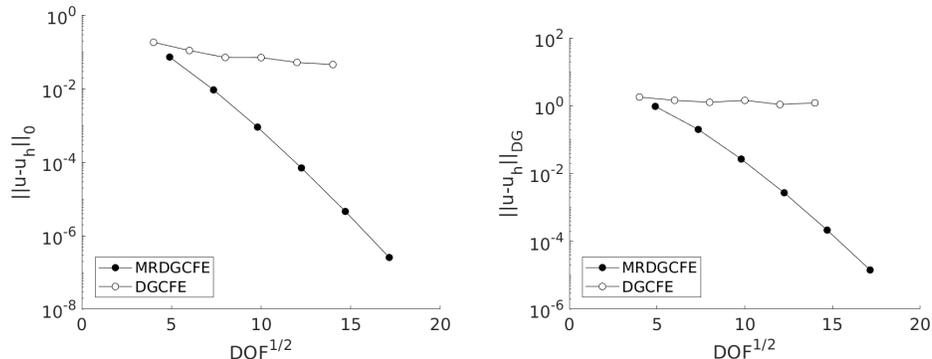
Figure 5: Results for the problem with $x_0 = 3/4$. (left) L^2 norm of the error. (right) DG norm of the error.

coarse mesh in this experiments is always the 2×2 structured mesh and p varying from 1 to 6.

In Figures 5, 6 and 7 we reported the behaviour of the errors measured in the L^2 and DG norm for both the MRDGCFE and the DGCFE for the three considered values of x_0. Compared to previous plots, these are semi-log plots showing the convergence rate close to exponential for the MRDGCFE method. This is understandable, thanks to the decomposition of composite elements according to the regions $\mathcal{R}_i$, ensuring that in the support of each composite element the solution u is smooth. Therefore increasing p we obtain exponential convergence of the method.

Remark 5.1. *For this problem, the interface between the regions $\mathcal{R}_i$ can be described using structured meshes. Due to the simplicity of the problem, the DGCFE method is equivalent to the SIPDG method and all the results apply as well.*

5.2. Regions with smooth interface

In this section, we consider problem (11) with the two regions where coefficient $\mathcal{A}$ assumes different values separated by a smooth curve. The domain Ω is $[0,1]^2$ with $\mathcal{A} = 1$ within the circle of centre $(0.5, 0.5)$ and radius 0.25 and with $\mathcal{A} = 100$ outside, see Figure 8(left). For this problem $f(x, y) = 1$ and $g(x, y) = 0$. The true solution of this problem is not known, but using the error estimator η a good approximation of the solution is computed. The fine level mesh $\mathcal{T}_{h_\ell}$ is an unstructured mesh of triangles

19
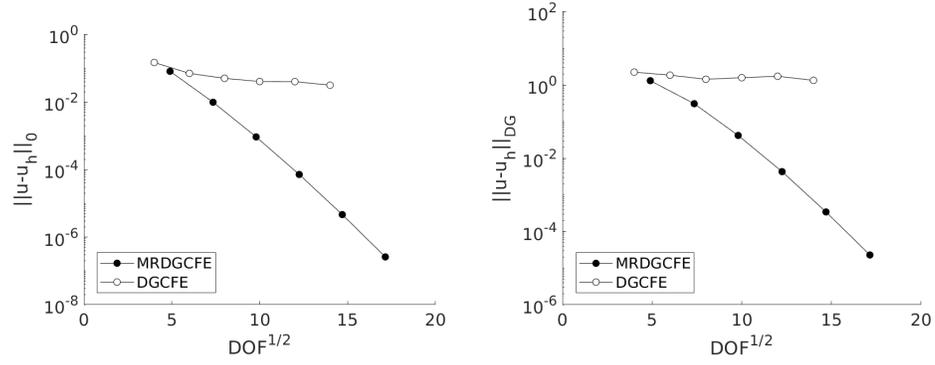
Figure 6: Results for the problem with $x_0 = 11/16$. (left) L^2 norm of the error. (right) DG norm of the error.
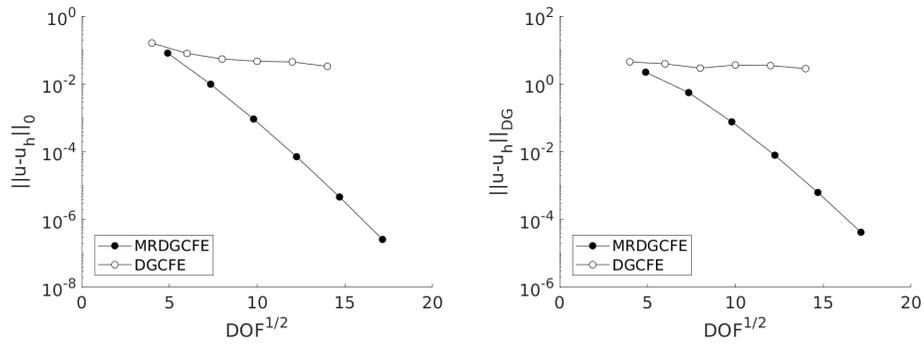
Figure 7: Results for the problem with $x_0 = 45/64$. (left) L^2 norm of the error. (right) DG norm of the error.

containing 387804 elements. Such a large number of elements is necessary to describe very accurately the interface between the two regions. Moreover, the edges of the elements in $\mathcal{T}_{h_\ell}$ are bended to for the geometry. The coarse level meshes $\mathcal{T}_{\mathrm{CFE}}$ are constructed from a series of structured meshes of square elements. This series of structured meshes are constructed using h-adaptivity and starting from a structured mesh of 8×8 square elements. It is important to point out that the CFEs in the $\mathcal{T}_{\mathrm{CFE}}$ meshes are defined as the aggregations of the fine triangular elements with centres laying inside the coarse square elements. Therefore, the shapes of the CFEs in the $\mathcal{T}_{\mathrm{CFE}}$ meshes are the resulting shapes from the aggregation of the fine level elements and they may not be square elements any more. For simplicity, in all figures, we still represent the CFEs as squares. As explained in [4], this is the most general setting when the coarse level and the fine level are not nested, the coarse level is only used to describe the topology of CFE mesh. In [4] is also explained that to construct correctly the coarse level finite element space, the polynomial space on each fine level elements must contain the polynomial space of the coarse father element. Since we use $\mathbb{Q}_1$ CFEs, we need to use the $\mathbb{Q}_1$ polygonal space also on the triangular elements on the fine mesh. This is not a problem since both the fine and the coarse finite element spaces are discontinuous Galerkin spaces and no continuity is required along the edges of the meshes. As for the previous example, the $\mathcal{T}_{\mathrm{CFE}}^{\mathrm{disc}}$ meshes are constructed from the $\mathcal{T}_{\mathrm{CFE}}$ meshes using the procedure described in Section 3.

In Figure 8(right) the convergence of the error estimator for the MRDGCFE method and the DGCFE method are reported. Even if the piecewise regions of coefficient $\mathcal{A}$ are never resolved exactly on any of the $\mathcal{T}_{\mathrm{CFE}}$ meshes, the decay of the error estimator for the MRDGCFE method looks consistent and better than the DGCFE method.

This can also be seen visually comparing the solutions of the MRDGCFE method and the DGCFE method computed on the final adapted meshes, see Figure 9. The solution computed with the MRDGCFE method is much more neat along the boundary of the inner region.

In Figure 10 the initial mesh and the values of the error estimator for the MRDGCFE method on each element is reported. The coarse level elements intersecting the interface are the ones with higher values.

In Figures 11 and 12 the third and fifth adapted meshes are reported for the MRDGCFE method together with the values of the error estimator for each element. After a few iterations of the adaptive procedure, high values appears not only in elements along the interface and refined elements appear
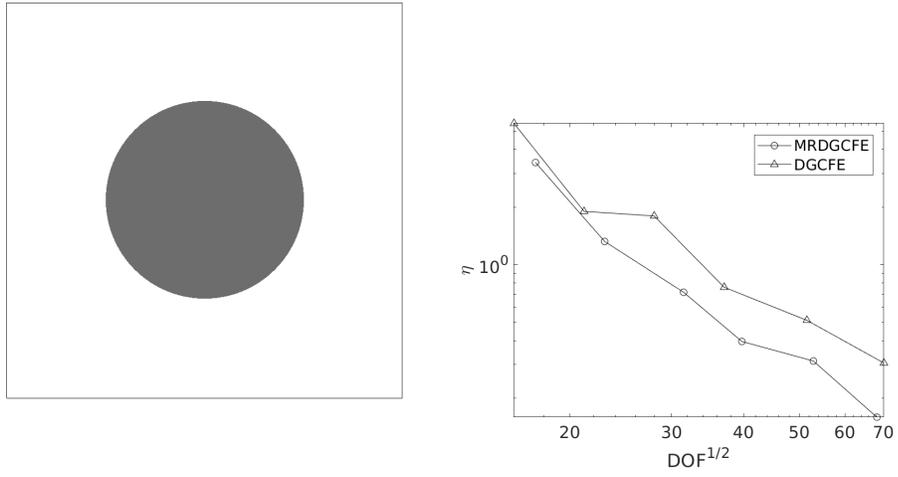
Figure 8: (left) Regions of definition for coefficient $\mathcal{A}$. (right) Convergence of the error estimator η using adaptive h-refinement for the MRDGCFE and the DGCFE method.
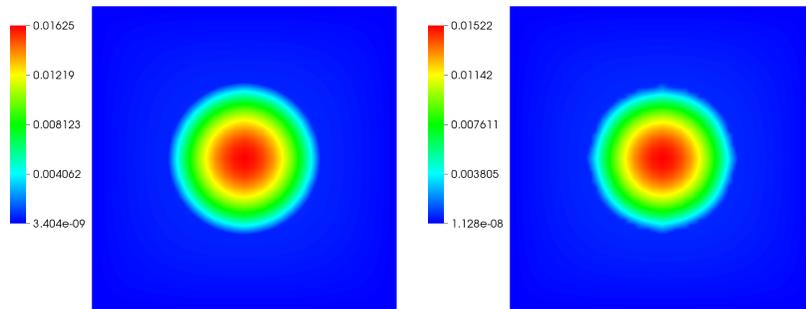
Figure 9: (left) Solution on the final adapted mesh of the MRDGCFE method. (right) Solution on the final adapted mesh of the DGCFE method..

22
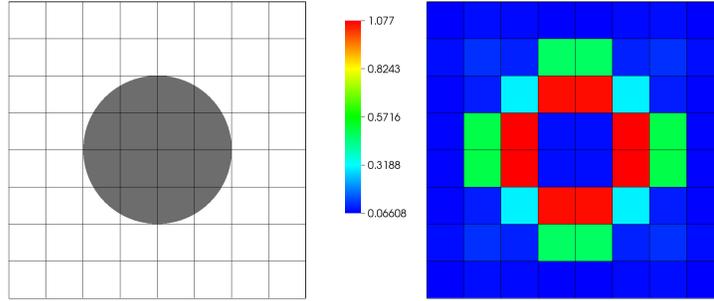
Figure 10: (left) Initial coarse level mesh. (right) Error estimator values on the initial mesh.

in different parts of the mesh. This is normal because locally refining the elements has the effect to reduce locally the values of the error estimator, so after few iterations other less refined parts of the mesh show the highest values for the estimator.

Similarly to what done in the previous section, we now compare the MRDGCFE method and the DGCFE method on the same problem using p-adaptivity. In this case, the initial polynomial order of both methods is 1 and the structured mesh of 8×8 square elements. Then the adaptive method decides automatically on what elements to increase the value of p.

In Figure 13 we reported the convergence of the error estimator for the MRDGCFE method and the DGCFE method, clearly as the MRDGCFE method outperforms the DGCFE method.

5.3. Problem with meso-structure

In this section, we consider problem (11) with regions where coefficient $\mathcal{A}$ assumes different values forming a meso-structure. The true solution of this problem is not known, but using the error estimator η a good approximation of the solution is computed. For this problem $g(x, y) = 0$ and with $f(x, y) = e^{\frac{-r(x,y)^2}{0.02^2}}$ where $r(x, y)$ is the distance of the point (x, y) from the centre of the domain $(0.5, 0.5)$. f is defined in such a way to concentrate the solution around the centre of the domain. The domain Ω is $[0, 1]^2$ with $\mathcal{A} = 1$ outside the white regions in Figure 14(left) and $\mathcal{A} = 100$ inside the regions. Such a complicated structure resembles the geometry of the photonic crystal fibre
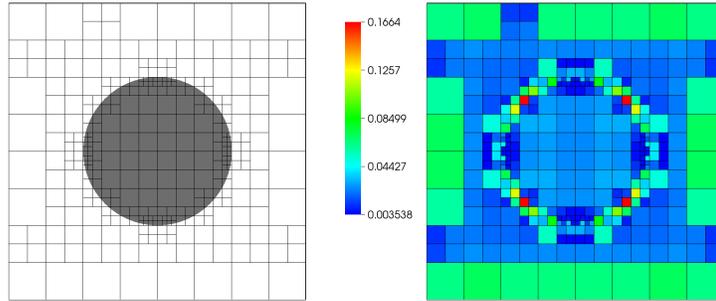
Figure 11: (left) Third mesh in the h-adaptive sequence. (right) Error estimator values on the third mesh.
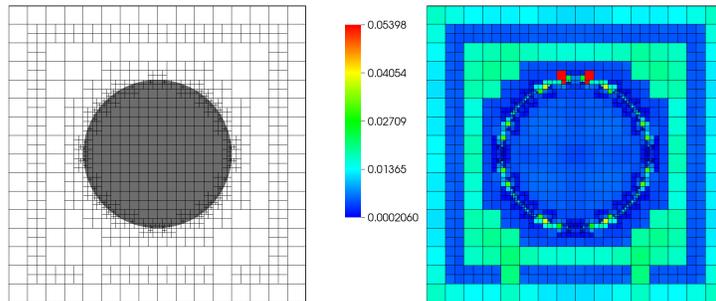
Figure 12: (left) Fifth mesh in the h-adaptive sequence. (right) Error estimator values on the fifth mesh.
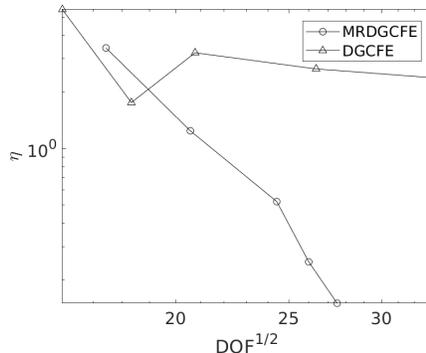
Figure 13: Convergence of the error estimator η using adaptive p-refinement for the MRDGCFE and the DGCFE method.

with a central defect [21]. The initial fine level mesh $\mathcal{T}_{h_\ell}$ is fine enough to resolve correctly the geometries of all regions. As before, h-adaptivity is applied in such a way that if necessary, also the fine level mesh is refined for compatibility with the coarse level mesh. The initial coarse level mesh is a structured mesh $\mathcal{T}_{\text{CFE}}$ of 3×3 elements, see Figure 15(left). As before the initial $\mathcal{T}_{\text{CFE}}^{\text{disc}}$ mesh is constructed from the $\mathcal{T}_{\text{CFE}}$ mesh.

In Figure 14(right) the convergence of the error estimator is reported. For this example, as in the previous one, the decay of the error estimator looks consistent even when the coarse level mesh is too coarse to resolve the interface geometry. The star indicates the value of the error estimator computed using the SIPDG method on the coarsest mesh that resolves the meso-structure. The plot suggests a possible usage of the MRDGCFE method to compute quickly approximation of solutions for complicated problems. For example, the MRDGCFE method can test quickly several different configurations of the meso-structure which could have applications for optimisation. In Figure 15 the initial mesh and the values of the error estimator for each element is reported. In Figures 16 and 17, the seventh and fifteenth adapted meshes are reported together with the values of the error estimator for each element. On the seventh mesh, some coarse level elements away from the central defect are still too coarse to capture the correct shape of the inclusions, nevertheless, the approximation looks good in the convergence plot for the error estimator. On the fifteenth mesh, the central region is heavily refined, since the solution is concentrated there. This is necessary to have a
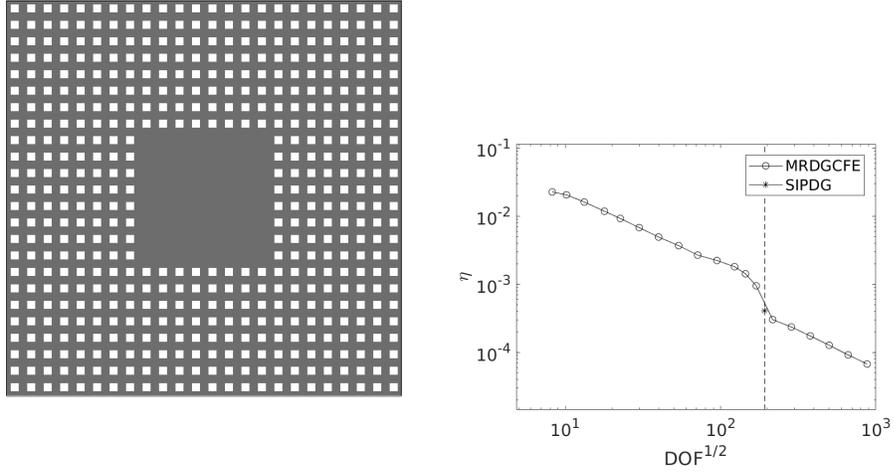
Figure 14: (left) Regions of definition for coefficient $\mathcal{A}$. (right) Convergence of the error estimator η using adaptive h-refinement.
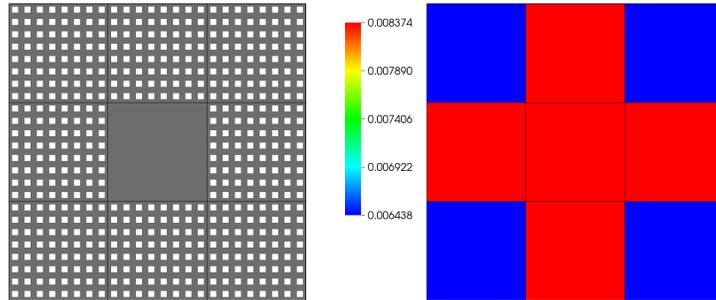
Figure 15: (left) Initial coarse level mesh. (right) Error estimator values on the initial mesh.
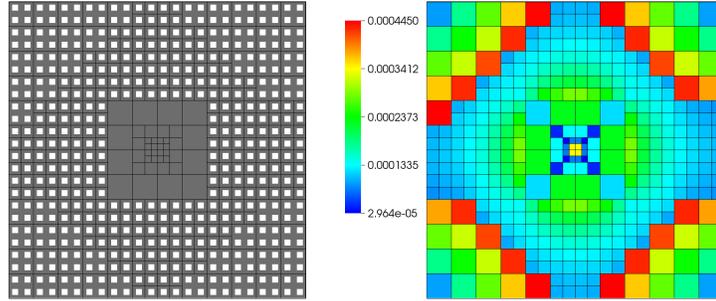
Figure 16: (left) Seventh mesh in the h-adaptive sequence. (right) Error estimator values on the seventh mesh.

very good overall approximation.

6. Conclusions

In this paper, we have presented the MRDGCFE method to solve elliptic PDE problems with coefficients with a fine scale of discontinuities. The method shows an improved efficiency compared to standard finite element methods and the DGCFE method. We have also shown how to use the method with an a posteriori error estimator to drive the adaptivity. The resulting method could be very useful for a variety of engineering problems since the error estimator can be used to decide when the solution is accurate enough for engineering purposes, as shown in Section 5.3, even if the mesh is not fine enough to describe the features of the problem resulting in a valuable gain computationally speaking.

We developed this method with two applications in mind that are composite materials and photonic crystals. The MRDGCFE method combines very well with results from recent papers to tackle the two mentioned problems. In particular, the MRDGCFE method could be used to solve problems involving composite materials combining it with the error estimator presented in [7]. Similarly, combining the MRDGCFE with DGCFE method for eigenvalues presented in [15] could result in an efficient numerical method for photonic crystal applications.
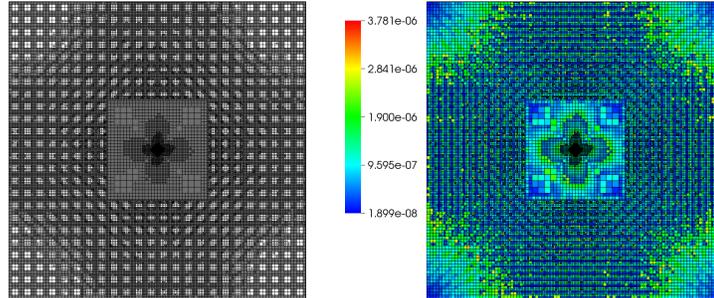
Figure 17: (left) Fifteenth mesh in the h-adaptive sequence. (right) Error estimator values on the fifteenth mesh.

References

[1] Jorg E. Aarnes, Stein Krogstad, and Knut-Andreas Lie. A Hierarchical Multiscale Method for Two-Phase Flow Based upon Mixed Finite Elements and Nonuniform Coarse Grids. *Multiscale Modeling & Simulation*, 5(2):337–363, January 2006.

[2] Jrg E. Aarnes, Stein Krogstad, and Knut-Andreas Lie. Multiscale mixed/mimetic methods on corner-point grids. *Computational Geosciences*, 12(3):297–315, September 2008.

[3] A. Abdulle and A. Nonnenmacher. Adaptive finite element heterogeneous multiscale method for homogenization problems. *Computer Methods in Applied Mechanics and Engineering*, 200(37-40):2710–2726, September 2011.

[4] P. Antonietti, S. Giani, and P. Houston. hp-version composite discontinuous Galerkin methods for elliptic problems on complicated domains. *SIAM Journal on Scientific Computing*, 35(3):A1417–A1439, 2013.

[5] D. Arnold, F. Brezzi, B. Cockburn, and L. Marini. Unified Analysis of Discontinuous Galerkin Methods for Elliptic Problems. *SIAM Journal on Numerical Analysis*, 39(5):1749–1779, January 2002.

[6] Marsha Berger and Michael Aftosmis. Progress Towards a Cartesian Cut-Cell Method for Viscous Compressible Flow. In *50th AIAA*

28

Aerospace Sciences Meeting including the New Horizons Forum and
Aerospace Exposition, Nashville, Tennessee, January 2012. American Institute of Aeronautics and Astronautics.

[7] R. E. Bird, W. M. Coombs, and S. Giani. A posteriori discontinuous galerkin error estimator for linear elasticity. *Applied mathematics and computation.*, 344-345:78–96, March 2019.

[8] Franois Bouchon, Thierry Dubois, and Nicolas James. A second-order cut-cell method for the numerical simulation of 2d flows past obstacles. *Computers & Fluids*, 65:80–91, July 2012.

[9] Erik Burman, Susanne Claus, Peter Hansbo, Mats G. Larson, and Andr Massing. CutFEM: Discretizing geometry and partial differential equations: DISCRETIZING GEOMETRY AND PARTIAL DIFFERENTIAL EQUATIONS. *International Journal for Numerical Methods in Engineering*, 104(7):472–501, November 2015.

[10] Erik Burman, Peter Hansbo, and Mats G. Larson. A stabilized cut finite element method for partial differential equations on surfaces: The LaplaceBeltrami operator. *Computer Methods in Applied Mechanics and Engineering*, 285:188–207, March 2015.

[11] Le Duan, Xiaowen Wang, and Xiaolin Zhong. A high-order cut-cell method for numerical simulation of hypersonic boundary-layer instability with surface roughness. *Journal of Computational Physics*, 229(19):7207–7237, September 2010.

[12] Daniel Elfverson. A discontinuous Galerkin multiscale method for convection-diffusion problems. *arXiv:1509.03523 [math]*, September 2015. arXiv: 1509.03523.

[13] Alexandre Ern, Annette F. Stephansen, and Martin Vohralk. Guaranteed and robust discontinuous Galerkin a posteriori error estimates for convection-diffusion-reaction problems. *J. Comput. Appl. Math.*, 234(1):114–130, 2010.

[14] Stefano Giani. hp-adaptive composite discontinuous Galerkin methods for elliptic eigenvalue problems on complicated domains. *Applied Mathematics and Computation*, 267:604–617, 2015.

[15] Stefano Giani. Solving elliptic eigenvalue problems on polygonal meshes using discontinuous galerkin composite finite element methods. *Applied mathematics and computation.*, 267:618–631, September 2015.

[16] Stefano Giani and Paul Houston. Goal-oriented adaptive composite discontinuous galerkin methods for incompressible flows. *J. Computational Applied Mathematics*, 270:32–42, 2014.

[17] Stefano Giani and Paul Houston. hp-adaptive composite discontinuous Galerkin methods for elliptic problems on complicated domains. *Numerical Methods for Partial Differential Equations*, 30(4):1342–1367, 2014.

[18] Peter Hansbo, Mats G. Larson, and Sara Zahedi. Characteristic cut finite element methods for convectiondiffusion problems on time dependent surfaces. *Computer Methods in Applied Mechanics and Engineering*, 293:431–461, August 2015.

[19] Peter Hansbo, Mats G. Larson, and Sara Zahedi. A cut finite element method for coupled bulk-surface problems on time-dependent domains. *Computer Methods in Applied Mechanics and Engineering*, 307:96–116, August 2016.

[20] Patrick Henning, Axel Må lqvist, and Daniel Peterseim. A localized orthogonal decomposition method for semi-linear elliptic problems. *ESAIM: Mathematical Modelling and Numerical Analysis - Modélisation Mathématique et Analyse Numérique*, 48(5):1331–1349, 2014.

[21] John Joannopoulos, Steven Johnson, Joshua Winn, and Robert Meade. *Photonic Crystals: Molding the Flow of Light.* Princeton University Press, Singapore, 2nd revised edition edition, 2008.

[22] Stein Krogstad, Knut-Andreas Lie, Halvor Moll Nilsen, Jostein Roald Natvig, B. Skaflestad, and J. Espen Aarnes. A Multiscale Mixed Finite Element Solver for Three Phase Black Oil Flow. In *SPE Reservoir Simulation Symposium*, The Woodlands, Texas, 2009. Society of Petroleum Engineers.

[23] M. Oleksy and W. Cecot. Estimation of computational homogenization error by explicit residual method. *Computers & Mathematics with Applications*, 66(12):2504–2516, January 2014.

552 [24] Maxim A. Olshanskii, Arnold Reusken, and Jrg Grande. A Finite El-
553 ement Method for Elliptic Equations on Surfaces. *SIAM Journal on*
554 *Numerical Analysis*, 47(5):3339–3358, January 2009.

555 [25] J. A. Sethian. *Level Set Methods and Fast Marching Methods: Evolv-*
556 *ing Interfaces in Computational Geometry, Fluid Mechanics, Computer*
557 *Vision, and Materials Science ... on Applied and Computational Math-*
558 *ematics).* Cambridge University Press, 2 edition, June 1999.

559 [26] E. M. Stein. *Singular Integrals and Differentiability Properties of Func-*
560 *tions.* Princeton, University Press, Princeton, N.J., 1970.

561 [27] P G Tucker and Z Pan. A Cartesian cut cell method for incompressible
562 viscous ow. page 16, 2000.

563 [28] Lei Zhang, Li-Qun Cao, and Xin Wang. Multiscale finite element algo-
564 rithm of the eigenvalue problems for the elastic equations in composite
565 materials. *Computer Methods in Applied Mechanics and Engineering*,
566 198(33-36):2539–2554, July 2009.